

Research Paper

Entropy Production Due to Conjugate Natural Convection in a Nanofluid-Filled Enclosure With a Stepped Wall

Abd el malik BOUCHOUCHA¹*, Hakan F. OZTOP²), Rachid BESSAÏH³),
Nidal ABU-HAMDEH⁴)

¹) *Department of Science and Technology, University of Mila*
Algeria

²) *Department of Mechanical Engineering, Technology Faculty, Firat University*
Elazig, Turkey

³) *LEAP Laboratory, Department of Mechanical Engineering, Faculty of Sciences Technology*
University Frères Mentouri-Constantine
Algeria

⁴) *Mechanical Engineering Department, Faculty of Engineering, King Abdulaziz University*
Jeddah, Saudi Arabia

*Corresponding Author e-mail: bouchoucha.malik@gmail.com

The main aim of this paper is to improve the heat transfer in a square cavity with a body at the left wall filled with a Al_2O_3 /water nanofluid for different geometries. Numerous simulation experiments are conducted. A relative temperature is maintained at the vertical and top horizontal walls while the bottom wall is warm. The finite volume approach is considered to resolve the equations governing the thermal transfer flow in the physical domain based on the SIMPLER algorithm. In this study, different values of the following parameters are considered: Rayleigh number ($10^4 \leq \text{Ra} \leq 10^5$) and solid volume fraction ($0 \leq \phi \leq 0.1$) of nanoparticles (NPs). Parameters, such as the Rayleigh (Ra) and Bejan (Be) numbers, thermal conductivity, body's dimensions, and NPs volume fraction, which directly affect the entropy generation and heat transfer rate, are studied in a particular way. The obtained results show that entropy generation goes ahead with the Ra increase and inverse to the solid volume fraction increase. One can notice that the heat transfer has a proportional relation with ϕ and Ra.

Keywords: entropy generation; natural convection; nanofluids; cavity; wall.

NOTATIONS

C_P – specific heat [$\text{J} \cdot \text{kg}^{-1} \cdot \text{K}^{-1}$],

K – thermal conductivity [$\text{W} \cdot \text{m}^{-1} \cdot \text{K}^{-1}$],

L – cavity length [m],

Nu_s – local Nusselt number along the heat source,

- Nu_m – average Nusselt number,
- U, V – dimensionless velocity components,
- x, y – Cartesian coordinates [m],
- X, Y – dimensionless coordinates ($x/L, y/L$),
- P – dimensionless pressure,
- G – gravitational acceleration [m/s^2],
- Ra – Rayleigh number ($g\beta\Delta TL^3/\nu_f\alpha_f$),
- S_{total} – total entropy generation,
- S_f – entropy generation due to friction,
- Be – Bejan number,
- S_{th} – entropy generation due to heat transfer.

Greek symbols

- α – thermal diffusivity [$m^2 \cdot s^{-1}$],
- β – thermal expansion coefficient [K^{-1}],
- φ – solid volume fraction,
- θ – dimensionless temperature,
- μ – dynamic viscosity [$kg \cdot m^{-1} \cdot s^{-1}$],
- ν – kinematic viscosity [$m^2 \cdot s^{-1}$],
- ρ – density [$kg \cdot m^{-3}$].

Subscriptions

- b – length of the body at the top wall,
- h – lower part body height,
- a – length of the body at the bottom,
- P – nanoparticle,
- f – fluid (pure water),
- nf – nanofluid,
- c – cold.

1. INTRODUCTION

Numerous researchers have studied laminar natural convection in cavities. Due to useful engineering purposes, such as removing heat from electrical apparatus, solar collectors, etc., several research papers have focused on improving natural convection in cavities by adding nanofluids (ALLOUI *et al.* [1], ZHANG *et al.* [2], JOU and TZENG [3] and HERIS *et al.* [4]). ABU-NADA [5] dealt with the entropy generation in his study on a backward-facing step subjected to bleeding conditions. This study concluded that the maximum entropy generation number (Ns) values are at the bottom wall (inside the primary recirculation zone) and the leading edge of the top wall, and high values for the Be number are on the top and bottom walls. KIM and BAEK [6] dealt with the influence of radiation on the compressible turbulent flow. This study found that the radia-

tive heat flux played some role only in the recirculating zone. GUERRERO and COTTA [7] presented the flow behavior in a backward-facing step using a benchmark integral transform technique. BENARD *et al.* [8], based on the dielectric barrier discharge (DBD) plasma actuator, investigated the coherent structure dynamics control on a backward-facing step. The natural convection evolution in a cavity stimulated by a heated backward step was studied by CHANG and TSAY [9] and RAMŠAK [10]. NIEMANN and FRÖHLICH [11] studied the effect of buoyancy force on the backward-facing step in the presence of heat transfer; the results of their study contributed to understanding of buoyancy force effect on turbulent heat transfer in the considered regime.

XU *et al.* [12] presented an experimental study that aimed to optimize the flow field control of a backward-facing step. For this purpose, a synthetic jet device was developed. KHERBEET *et al.* [13] presented an experimental work to reveal the heat transfer and nanofluid flow evolution. The obtained experimental results agree with those presented in the literature. MRAMOR *et al.* [14] discussed the laminar backward-facing step flow under magnetic field conditions. STATNIKOV *et al.* [15] dealt with wake flow modes in transonic backward-facing step geometry. The study on the heat convection of an Al_2O_3 /water nanofluid subjected to a magnetic field was presented in AGHAKHANI *et al.* [16] and AL-NAQI *et al.* [17]. The heat transfer rate was discussed under different conditions such as magnetic field strength, the Rayleigh number evolution, radiation parameter and NPs' concentration. BAGHSAZ *et al.* [18] studied the convection heat transfer behavior under NP sedimentation in a completely porous enclosure. A conductive heat transfer was obtained while natural convection and rotational flow decreased as formation of sediment layers at the bottom of the enclosure reduced the streamlines. BEZI *et al.* [19] studied the natural convection effect on the entropy generation for multiple nanofluids within a semi-annular cavity. The obtained results proved that with increasing φ and Ra the entropy generation is augmented.

BONDAREVA *et al.* [20] studied numerically the natural convection with the entropy generation in a partially heated open cavity with a Cu-water nanofluid. Their study showed that for high values of the Rayleigh number heat transfer improved and fluid flow reduced. CHO [21] investigated the heat transfer effect and entropy generation in a mixed convection flow in a wavy-wall enclosure. DOGONCHIA *et al.* [22] studied magnetic nanofluid natural convection in the porous cavity using control volume finite element method (CVFEM). DORMO-HAMMADIA *et al.* [23] optimized the heat transfer based on the entropy generation minimization method in a wavy channel. HASHIM *et al.* [24] studied the natural convection in a U-shaped CuO/water nanofluid filled cavity. KHAKRAH *et al.* [25] studied heat transfer and nanofluid flow during natural convection based on the thermal lattice Boltzmann in a rectangular enclosure with a sinu-

soidal wall. RAHIMI *et al.* [26, 27] investigated natural convection in H-shaped enclosure and entropy generation under different conditions.

SELIMEFENDIGIL and OZTOP [28] presented the analysis of natural convection of nanofluid in an inclined enclosure containing wavy shape conductive partition. Their study illustrates that higher values of Ra stand for the average Nusselt (Nu) number augmentation. On the other hand, the higher values of the Hartmann number stand for the average Nu number reduction. SHEIK-HOLESLAMI and OZTOP [29] studied an Fe_3O_4 -water nanofluid natural convection in a cavity with a sinusoidal surface cylinder subjected to an external magnetic field using the CVFEM. The obtained result shows that the thermal plume slanted to the left side because of the Lorentz forces. A high Hartmann number stands for a more effective impact of adding NPS. SHEREMET *et al.* [30] studied the natural convection of nanofluid in a curvy-walled cavity. The considered cavity contained an isothermal heater at one of its corners. The heat source in this cavity was obtained from the left bottom corners, and the cooling source was obtained from the top curvy part. Other walls were adiabatic. The single-phase nanofluid method was used to obtain the equivalent mathematical model. HASSAN *et al.* [32] studied the thermal energy and mass transport of shear-thinning fluid under the effects of low to high shear rate viscosity. SHAFIQ *et al.* [33] investigated the thermal energy and mass transport of shear-thinning fluid under the effects of low to high shear rate viscosity.

REDDY *et al.* [34] studied the radiation, velocity and thermal slips effect toward MHD boundary layer flow through heat and mass transport of Williamson nanofluid with porous medium. DHIF *et al.* [35] presented a thermal analysis of the solar collector cum storage system using hybrid nanofluids. MEBAREK-LOUDINA [36] studied the numerical modeling of the hydrodynamic stability in a vertical annulus with a heat source of different lengths. MEBAREK-LOUDINA [37] studied the convective heat transfer of titania nanofluids of different base fluids in a cylindrical annulus with a discrete heat source. CHABANI *et al.* [38] presented the numerical analysis of magnetic hybrid nano-fluid natural convective flow in an adjusted porous trapezoidal enclosure. MARZOUGUI *et al.* [39] studied the entropy generation and heat transport of Cu-water nano liquid in a porous lid-driven cavity through a magnetic field.

This paper presents the research of stable laminar natural convection in a cavity loaded with nanofluid. The authors have considered different geometries to get the influence of each Ra, Nf, thermal conductivity on total entropy generation, and the average Nusselt number. This study begins by introducing the principle of entropy generation and nanofluid into a square cavity. After that, we present the considered geometry and mathematical model. Then, the numerical method and code validation are tested in the third section to show the effectiveness of the considered code. Results and discussion are presented in

the fourth section. At the end of this study, a conclusion is given to outline the various findings.

2. GEOMETRY CONFIGURATION AND MATHEMATICAL MODELING

2.1. Problem statement

Figure 1 shows the considered geometry, which consists of a square cavity containing a body filled with nanofluid at its left wall. A relative temperature is maintained at the vertical and top horizontal walls while the bottom wall is hot. Since the base fluid is incompressible, the hypothesis of a Newtonian fluid, which fulfills the Boussinesq condition, the laminar flow and the nanofluids, is considered incompressible. Thermophysical properties of the nanofluid are constant, in opposition to density variation predicted by the Boussinesq hypothesis. The thermo-physiques properties are recapitulated in Table 1.

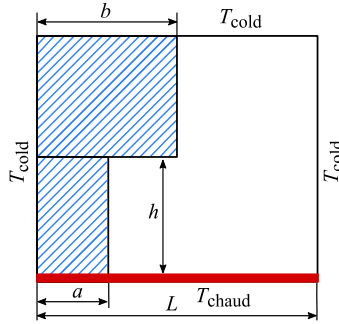


FIG. 1. Schematic for the physical model.

Table 1. Thermo-physical properties of pure water and NPs [31].

	ρ [kg · m ⁻³]	C_p [J · kg ⁻¹ · K]	k [W · m ⁻¹ · K ⁻¹]	$\beta \cdot 10^{-5}$ [K ⁻¹]	$\alpha \cdot 10^{-6}$ [m ² /s]
Pure water	997.1	4179	0.613	21	0.147
Alumina (Al ₂ O ₃)	3970	765	40	0.85	13.17

2.2. Modeling equations

The following equations present momentum, continuity and energy model for the laminar and stable state natural convection in a 2D square enclosure [31]:

$$(2.1) \quad \frac{\partial u}{\partial x} + \frac{\partial u}{\partial y} = 0,$$

$$(2.2) \quad u \frac{\partial u}{\partial x} + v \frac{\partial u}{\partial y} = \frac{1}{\rho_{nf}} \left[-\frac{\partial p}{\partial x} + \mu_{nf} \left(\frac{\partial^2 u}{\partial x^2} + \frac{\partial^2 u}{\partial y^2} \right) \right],$$

$$(2.3) \quad u \frac{\partial v}{\partial x} + v \frac{\partial v}{\partial y} = \frac{1}{\rho_{nf}} - \left[\frac{\partial p}{\partial x} + \mu_{nf} \left(\frac{\partial^2 v}{\partial x^2} + \frac{\partial^2 v}{\partial y^2} \right) + (\rho\beta)_{nf} g (T - T_C) \right],$$

$$(2.4) \quad u \frac{\partial T}{\partial x} + v \frac{\partial T}{\partial y} = \alpha_{nf} \left(\frac{\partial^2 T}{\partial x^2} + \frac{\partial^2 T}{\partial y^2} \right),$$

$$(2.5) \quad \frac{\partial^2 T}{\partial x^2} + \frac{\partial^2 T}{\partial y^2} = 0.$$

The nanofluid's efficient density is as follows:

$$(2.6) \quad \rho_{nf} = (1 - \phi) \rho_f + \phi \rho_p,$$

where ϕ denotes the NPs' solid volume fraction, and the thermal diffusivity of the nanofluid is given by:

$$(2.7) \quad \alpha_{nf} = k_{nf} / (\rho C_p)_{nf}.$$

The heat capacitance of the nanofluid could be expressed by:

$$(2.8) \quad (\rho C_p)_{nf} = (1 - \phi) (\rho C_p)_f + \phi (\rho C_p)_p.$$

The following equation permits to determine the nanofluid thermal expansion coefficient:

$$(2.9) \quad (\rho\beta)_{nf} = (1 - \phi) (\rho\beta)_f + \phi (\rho\beta)_p.$$

Brinkman specifies the nanofluid effective dynamic viscosity as follows [40]:

$$(2.10) \quad \mu_{nf} = \frac{\mu_f}{(1 - \phi)^{2.5}},$$

where k_{nf} is the nanofluid thermal conductivity presented in Eq. (2.11), according to Maxwell [41], for spherical NPs:

$$(2.11) \quad k_{nf} = k_f \left[\frac{(k_p + 2k_f) - 2\phi(k_f - k_p)}{(k_p + 2k_f) + \phi(k_f - k_p)} \right].$$

Dimensionless parameters are set up, in spite of making the equations model in a dimensionless form as:

$$(2.12) \quad \begin{aligned} X &= \frac{x}{L}, & Y &= \frac{y}{L}, & U &= \frac{uL}{\alpha_f}, \\ V &= \frac{vL}{\alpha_f}, & P &= \frac{pL^2}{\rho_{nf}\alpha_f^2}, & \theta &= \frac{T - T_C}{\Delta T (= T_H - T_C)}. \end{aligned}$$

Equations that govern dimensionless continuity, momentum and energy are given by:

$$(2.13) \quad \frac{\partial U}{\partial X} + \frac{\partial V}{\partial Y} = 0,$$

$$(2.14) \quad U \frac{\partial U}{\partial X} + V \frac{\partial U}{\partial Y} = -\frac{\partial P}{\partial X} + \frac{\mu_{nf}}{\rho_{nf}\alpha_f} \left(\frac{\partial^2 U}{\partial X^2} + \frac{\partial^2 U}{\partial Y^2} \right),$$

$$(2.15) \quad U \frac{\partial V}{\partial X} + V \frac{\partial V}{\partial Y} = -\frac{\partial P}{\partial Y} + \frac{\mu_{nf}}{\rho_{nf}\alpha_f} \left(\frac{\partial^2 V}{\partial X^2} + \frac{\partial^2 V}{\partial Y^2} \right) + \frac{(\rho\beta)_{nf}}{\rho_{nf}\beta_{nf}} \text{Ra Pr } \theta,$$

$$(2.16) \quad U \frac{\partial \theta}{\partial X} + V \frac{\partial \theta}{\partial Y} = \frac{\alpha_{nf}}{\alpha_f} \left(\frac{\partial^2 \theta}{\partial X^2} + \frac{\partial^2 \theta}{\partial Y^2} \right),$$

$$(2.17) \quad \frac{\partial \theta_f}{\partial X} = R_c \frac{\partial \theta_s}{\partial X}.$$

The Rayleigh number (Ra), Prandtl number (Pr), and thermal conductivity rate R_c are expressed respectively by:

$$(2.18) \quad \text{Ra} = \frac{g\beta_f L^3 (T_H - T_C)}{\nu_f \alpha_f}, \quad \text{Pr} = \frac{\nu_f}{\alpha_f}, \quad R_c = \frac{K_s}{K_f}.$$

2.3. Entropy generation model

The terms that quantify the entropy generation irreversibility presented in Eq. (2.19) are presented by:

- a character expressing the heat transfer,
- a character reflecting the viscous friction.

After that, the local entropy generation is given by:

$$(2.19) \quad s_{\text{gen}} = \frac{k_{nf}}{T_0^2} \left[\left(\frac{\partial T}{\partial x} \right)^2 + \left(\frac{\partial T}{\partial y} \right)^2 \right] + \frac{\mu_{nf}}{T_0} \left\{ 2 \left[\left(\frac{\partial u}{\partial y} \right)^2 + \left(\frac{\partial v}{\partial y} \right)^2 \right] + \left(\frac{\partial u}{\partial y} + \frac{\partial v}{\partial x} \right)^2 \right\},$$

where $T_0 = (T_H + T_C)/2$.

Based on the above introduced non-dimensional parameters, the dimensionless local entropy generation in Eq. (2.19) becomes:

$$(2.20) \quad S_{\text{gen}} = \frac{k_{nf}}{k_f} \left[\left(\frac{\partial \theta}{\partial x} \right)^2 + \left(\frac{\partial \theta}{\partial y} \right)^2 \right] + \varphi \left\{ 2 \left[\left(\frac{\partial U}{\partial X} \right)^2 + \left(\frac{\partial V}{\partial Y} \right)^2 \right] + \left(\frac{\partial U}{\partial Y} + \frac{\partial V}{\partial X} \right)^2 \right\}.$$

The irreversibility distribution rate φ is given by:

$$(2.21) \quad \varphi = \frac{\mu_{nf} T_0}{k_f} \left(\frac{\alpha_f}{L(T_H - T_C)} \right)^2.$$

Integrating the following equation in all computational domains, gives the dimensionless total entropy generation S_t :

$$(2.22) \quad S_t = \int S_{\text{gen}} \, dV.$$

The ratio between the entropy generation due to heat transfer and the total entropy generation is called the Bejan number and is expressed as [33]:

$$(2.23) \quad \text{Be} = \frac{S_{\text{gen},h}}{S_{\text{gen}}}.$$

2.4. Boundary conditions

The dimensionless boundary conditions are given by:

$$(2.24) \quad \begin{aligned} &\text{at } X = 0, \quad 0 \leq Y \leq 1 : U = V = 0, \quad \theta = 1, \\ &\text{at } X = 1, \quad 0 \leq Y \leq 1 : U = V = 0, \quad \theta = 0, \\ &\text{at } Y = 0, \quad 0 \leq X \leq 1 : U = V = 0, \quad \theta = 0, \\ &\text{at } Y = 1, \quad 0 \leq X \leq 1 : U = V = 0, \quad \theta = 0. \end{aligned}$$

2.5. Local and mean Nusselt numbers

The local Nusselt number is given by:

$$(2.25) \quad \text{Nu} = \frac{hL}{k_f},$$

where h denotes the heat transfer coefficient and it is given by:

$$(2.26) \quad h = -k_{nf} \left(\frac{\partial T}{\partial x} \right)_{\text{wall}} .$$

Based on the aforementioned non-dimensional variables, the local Nusselt number becomes

$$(2.27) \quad \text{Nu} = -\frac{k_{nf}}{k_f} \left(\frac{\partial \theta}{\partial X} \right)_{\text{wall}} .$$

As a final point, the mean Nusselt number Nu_m can be expressed as:

$$(2.28) \quad \text{Nu}_m = \frac{1}{A} \int \text{Nu} \, dA .$$

3. NUMERICAL METHOD

The control volume algorithm is considered to resolve equations Eqs. (2.13)–(2.16) with boundary conditions [42]. Simulation is via a FORTRAN code based on numerical procedure of SIMPLER [42] to treat the pressure-velocity coupling. The power-law scheme is adopted to treat convection terms when the energy balances are less than a specified accuracy value, i.e., 0.1%.

3.1. Grid independence study

Five grids with: 40×40 , 60×60 , 80×80 , 100×100 , and 120×120 nodes are used to obtain the best one. Table 2 gives the maximum values of Nu_m behavior in the function of grid size for the Al_2O_3 -water nanofluid, $\phi = 0.1$ and $\text{Ra} = 10^5$. In this table, one can notice that for the three grids of 80×80 , 100×100 , and 120×120 , a small change takes place in the calculated value. In addition, for 100×100 and 120×120 nodes, we observe that the variation of Nu_m is less than 0.00001. Despite the fact that the tests are carried out regarding numerical solution and the mesh, the grid chosen to complete calculations is the fourth one: 100×100 nodes.

Table 2. Grid independency properties (Al_2O_3 -water nanofluid, $\phi = 0.1$ and $\text{Ra} = 10^5$).

Grid	40×40	60×60	80×80	100×100	120×120
Nu_m	9.60801	10.60801	10.65801	10.66801	10.66802

3.2. Code validation

To show the numerical code's effectiveness, the obtained result is compared with Aminossadati and Ghasemi's results [31]. Figure 2a shows the dimensionless

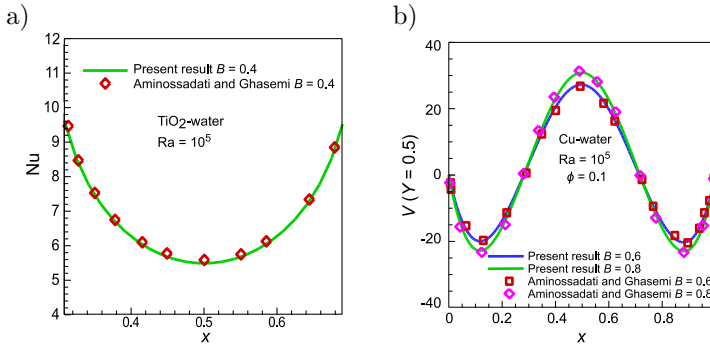


FIG. 2. Comparison of the obtained results to AMINOSSADATI and GHASEMI [31], at $Ra = 10^5$:
 a) local Nu number, b) the vertical velocity profile.

Nu comparison, whereas Fig. 2b shows the vertical velocity profile along the midsection of the enclosure for Cu-water nanofluid. It is clear that the obtained results show an excellent agreement with those presented in the literature.

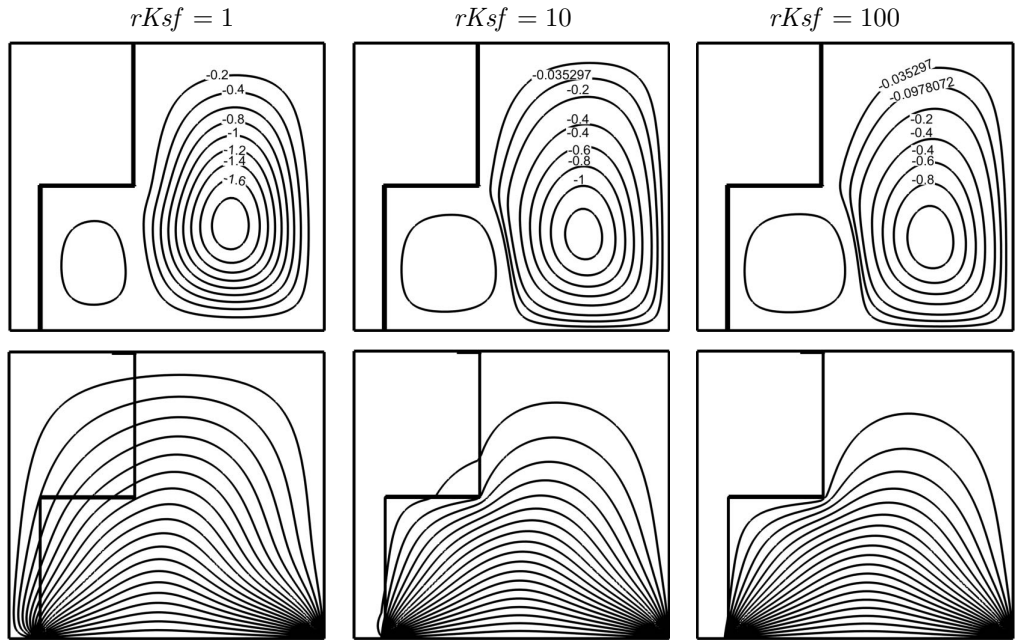
4. RESULTS AND DISCUSSION

Natural convection is affected by different parameters such as Ra , rate of thermal conductivity and different geometry shapes. In the simulation, aluminum NPs are dropped in water with a concentration of ($\phi_{\text{water}} = 0.9$, $\phi_{\text{Al}} = 0.1$).

Figure 3 shows the streamlines and isotherms for the nanofluid $\phi = 0.1$ and various Ra numbers, thermal conductivities and body dimensions. Let us note that the flow pattern consists of two counter-rotating cells for all configurations (Figs. 3–5). This movement of the fluid forms counter-rotating circulating cells within the enclosure. At $Ra = 10^4$, the streamlines show two vortices; the first big vortex in the vertical portion and the small one in the horizontal part for all thermal conductivity values. This is related mainly to the buoyancy force effect. Indeed, the fluid flow increases in the middle and decreases on the enclosure's side as a result of buoyant forces generated by fluid temperature differences. The fluid movement has a counter-rotating form in the enclosure. One can notice that the circulating cells' nature is changing according to Ra . For $Ra = 10^5$ and 10^6 , streamlines exhibit stronger flow patterns, and it is remarkable that the fluid flow is asymmetrical. Moreover, this asymmetry is accompanied by an augmentation in the flow intensity and a diminution in the size of two vortices, and we observe small cell in the cavity, which moves to the cavity's side.

The corresponding isotherms (Figs. 3–5) present asymmetry for all the cases. The isotherms are quasi-parallel to isothermal walls representing the predominance of heat conduction at a low $Ra = 10^4$ for all thermal conductivity values.

a) $\phi = 0.1, Ra = 10^4$



b) $\phi = 0.1, Ra = 10^5$

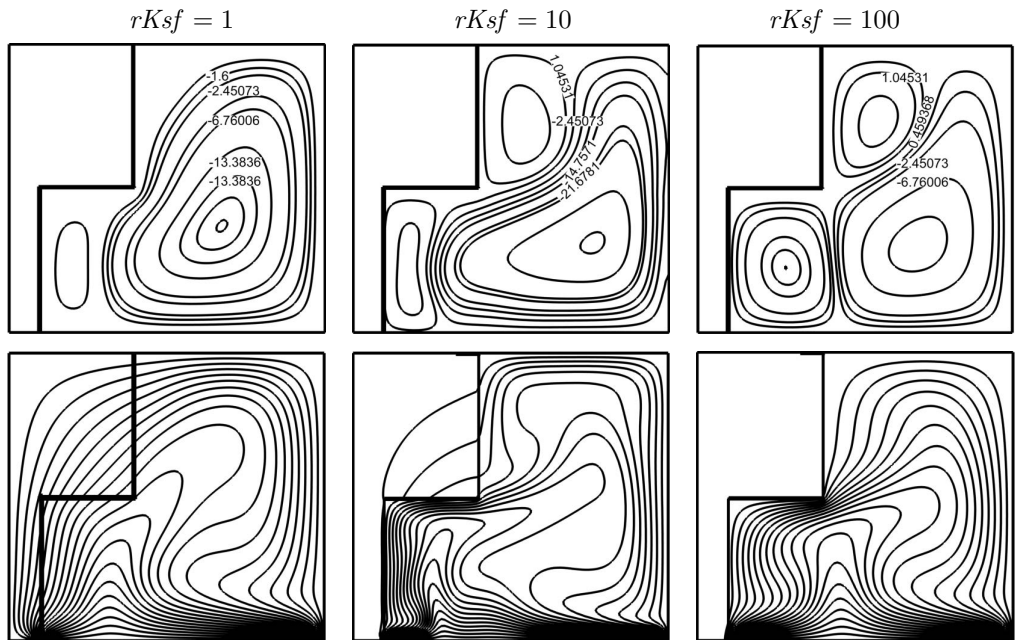


[FIG. 3ab]

c) $\phi = 0.1, Ra = 10^6$

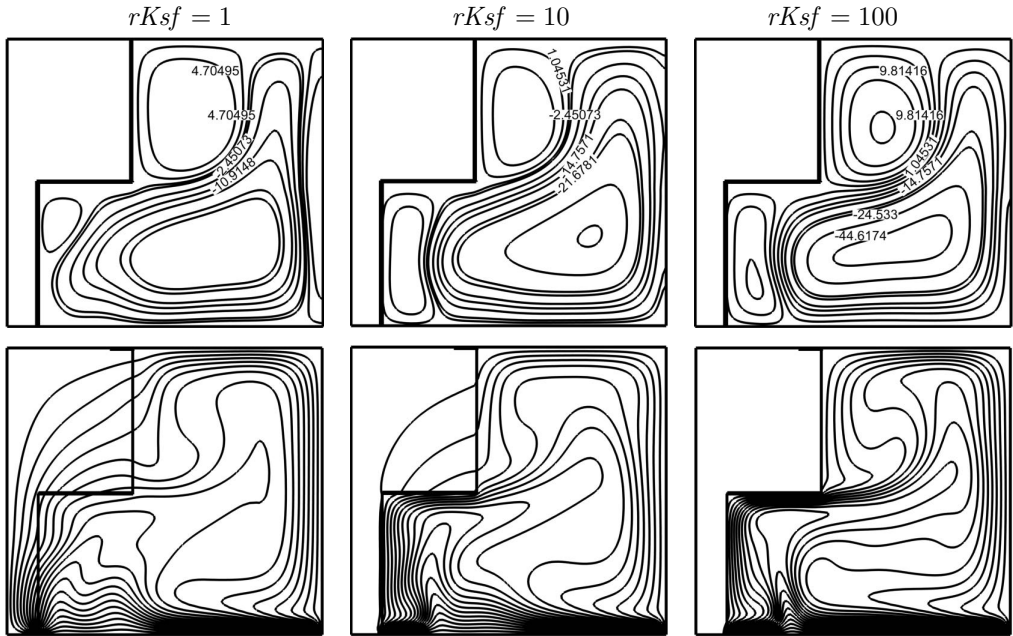
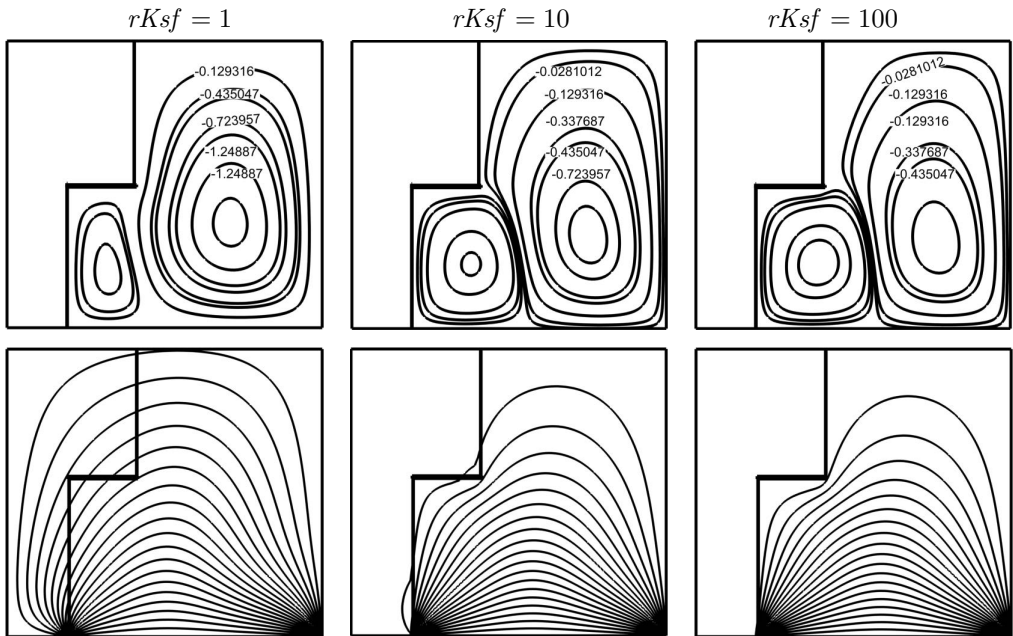


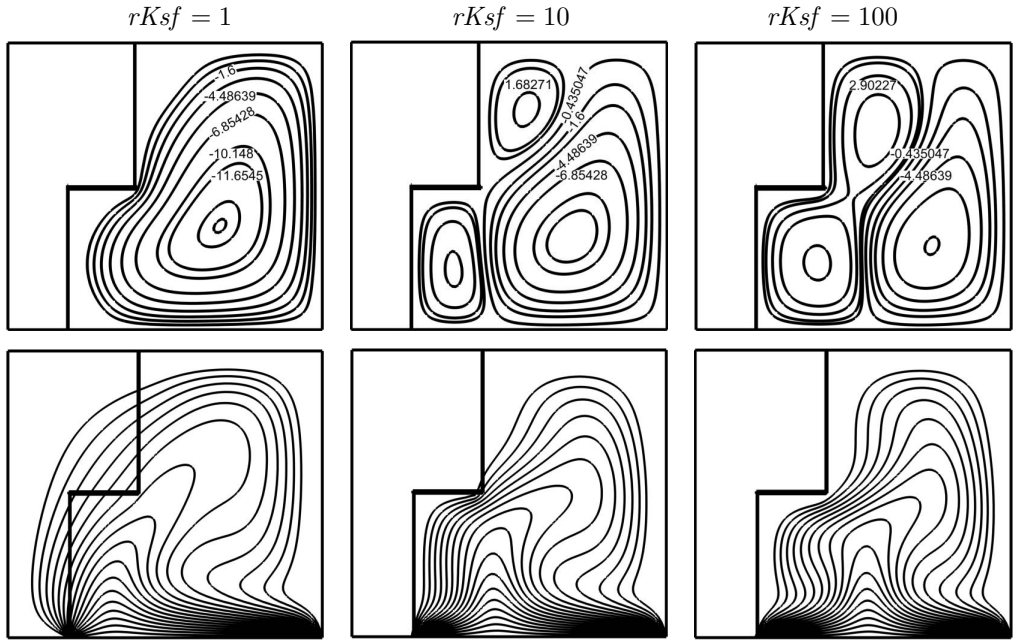
FIG. 3. Current function (up) and isotherms representation (down) for the loaded cavity under the condition of Al_2O_3 for case 1 ($a = 0.1, b = 0.4, h = 0.5$), $\phi = 0.1$, various $rKsf$ values, and $Ra = 10^4$ (a), $Ra = 10^5$ (b), and $Ra = 10^6$ (c).

a) $\phi = 0.1, Ra = 10^4$



[FIG. 4a]

b) $\phi = 0.1, Ra = 10^5$



c) $\phi = 0.1, Ra = 10^6$

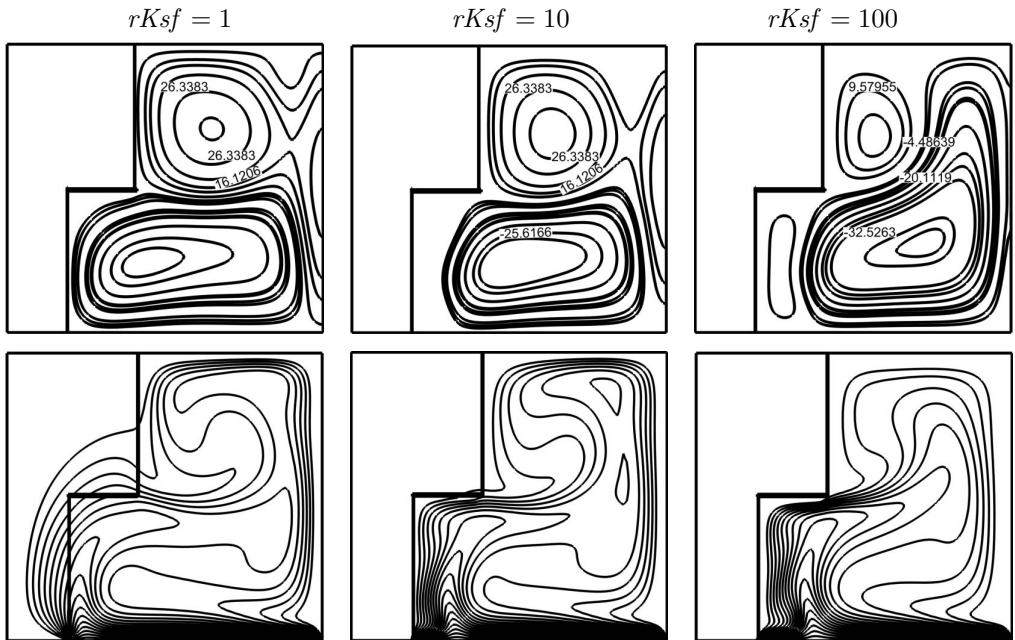
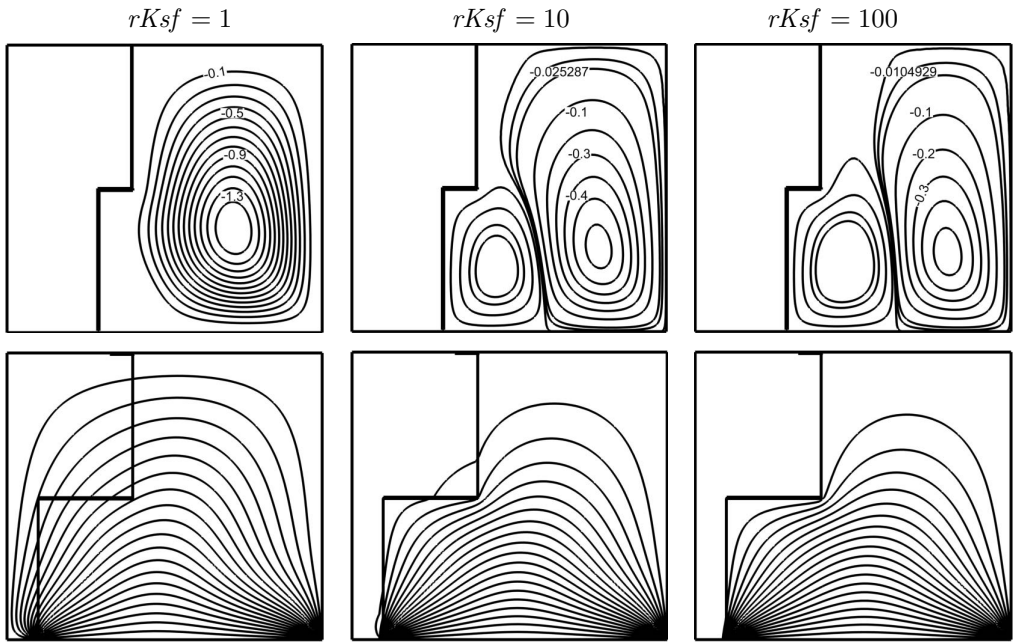
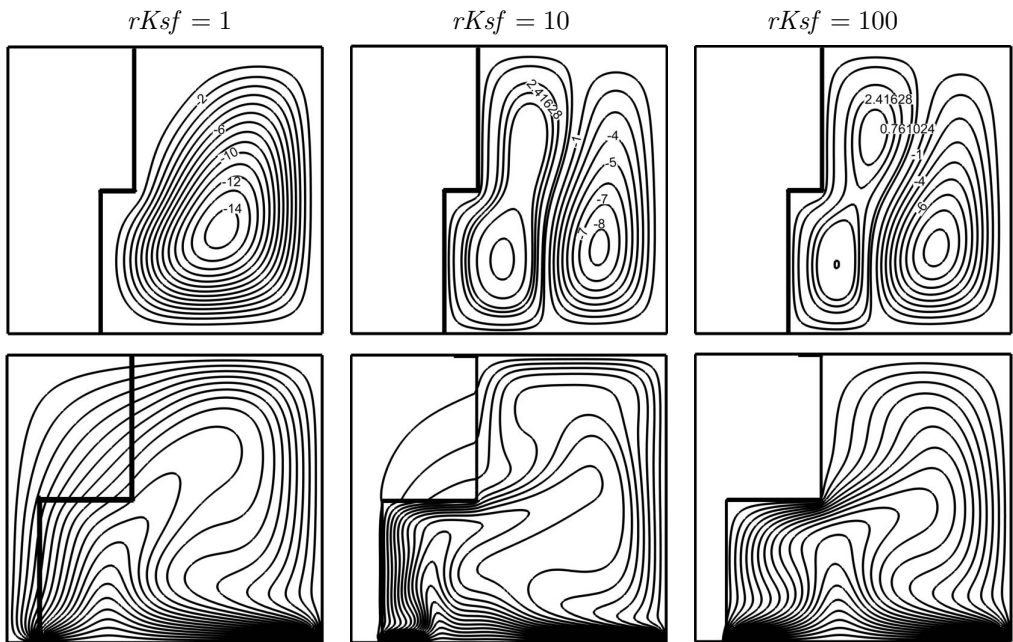


FIG. 4. Stream function (up) and isotherms representation (down) for the loaded cavity under the condition of Al_2O_3 , for case 2 ($a = 0.2, b = 0.4, h = 0.5$), $\phi = 0.1$, various $rKsf$ values, and $Ra = 10^4$ (a), $Ra = 10^5$ (b), and $Ra = 10^6$ (c).

a) $\phi = 0.1, Ra = 10^4$



b) $\phi = 0.1, Ra = 10^5$



[FIG. 5ab]

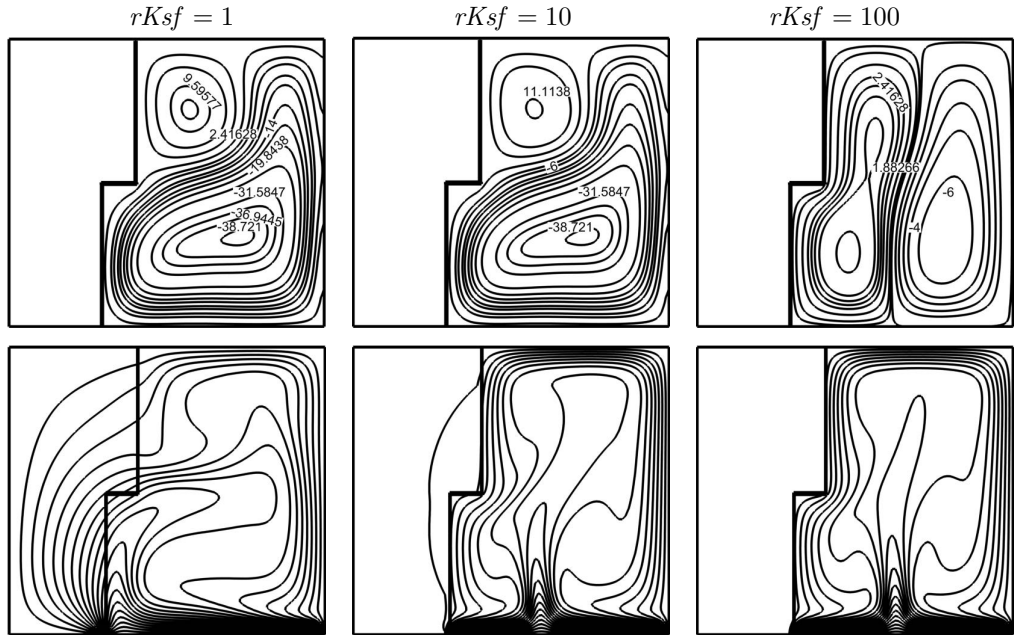
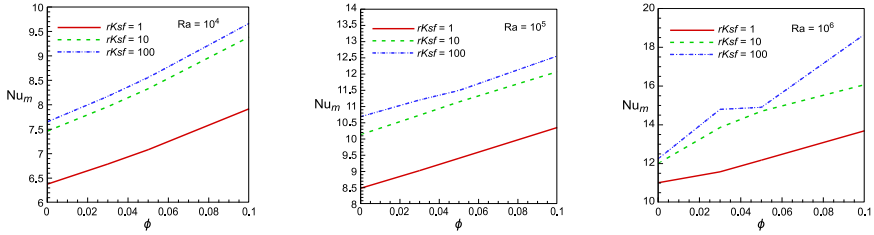
c) $\phi = 0.1$, $Ra = 10^6$ 

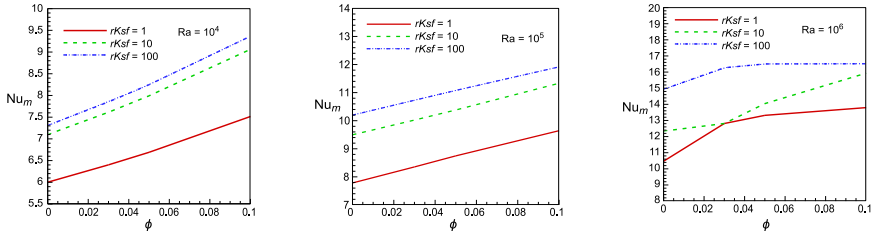
FIG. 5. Current function (up) and isotherms representation (down) for the loaded cavity under the condition of Al_2O_3 for case 3 ($a = 0.3$, $b = 0.4$, $h = 0.5$), $\phi = 0.1$, various $rKsf$ values, and $Ra = 10^4$ (a), $Ra = 10^5$ (b), and $Ra = 10^6$ (c).

Heat transfer within the enclosure occurs primarily as a consequence of conduction. For $Ra = 10^5$ and 10^6 , we notice the thermal boundary layer along the horizontal wall bottom and near the body. The isotherms have a heavy density close to the body and bottom wall. This fact leads to a heat transfer coefficient augmentation. The addition of NPs to pure water weakens the potency of the flow field; this reduction is more pronounced at small Ra (10^4). The thermal conductivity effect of NPs justifies the presence of NPs and their solid volume fraction. When the thermal conductivity ratio increases, the isotherm lines contract near the body and the bottom wall for all values of Ra . We notice that the best distribution is obtained when the heat source length is equal to case 1 ($a = 0.1$, $b = 0.4$, $h = 0.5$). Figure 6 demonstrates the Nu_m evolution concerning NPs volume fraction for various Ra numbers (10^4 – 10^6) at various thermal conductivities and different body dimensions. For all Ra values, the Nu_m increases as the volume fraction increases, and the conductive heat transfer increases by adding more NPs to the base fluid. On the other hand, the convective heat transfer is reduced because of lower velocity and higher density. While average heat transfer remains constant, the presence of the NPs has more effect on the heat transfer in the case of a small Ra number. At that point, the conduction mechanism has a major role. A stronger convection heat transfer

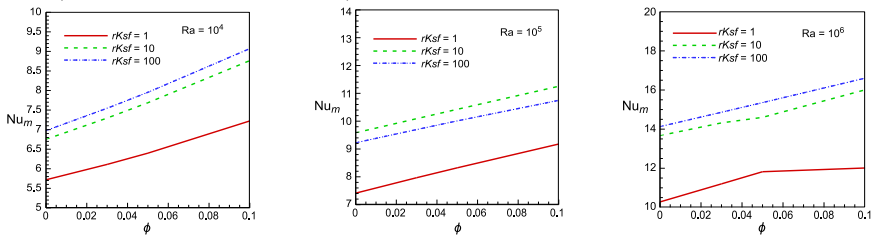
a) Case 1 ($a = 0.1, b = 0.4, h = 0.5$)



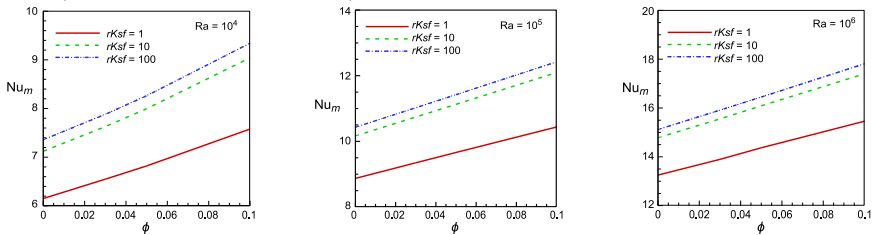
b) Case 2 ($a = 0.2, b = 0.4, h = 0.5$)



c) Case 3 ($a = 0.3, b = 0.4, h = 0.5$)



d) Case 4 ($a = 0.2, b = 0.1, h = 0.5$)



e) Case 5 ($a = 0.2, b = 0.3, h = 0.5$)

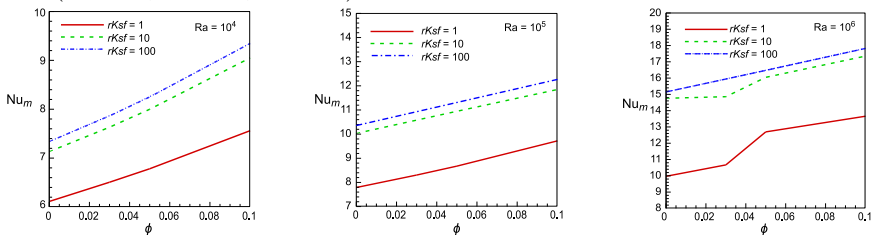
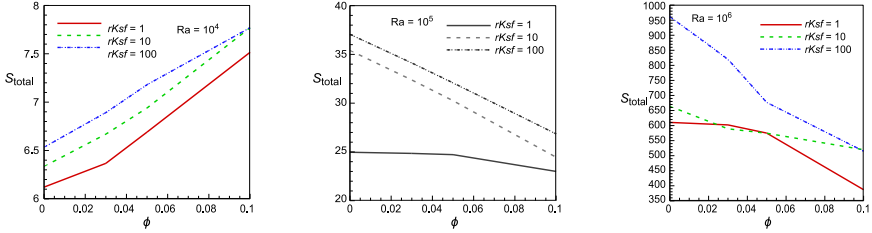


FIG. 6. Nu_m evolution with respect to solid volume fraction for various Ra , thermal conductivities and different geometries.

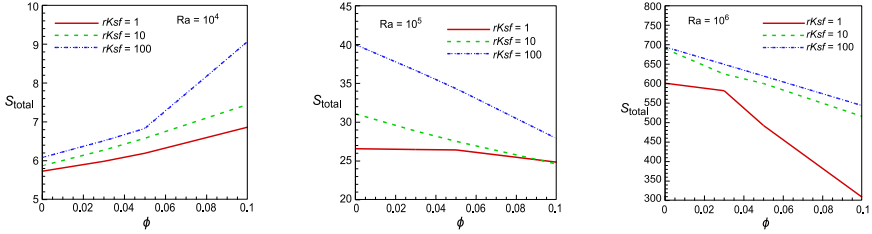
when $Ra > 10^4$ ameliorates the mean Nu number; besides, the mean Nu number enhancement is proportional to NPs presence and the increased Ra. The mean Nusselt number has a linear variation form in this case. This is due to the high buoyancy forces effects. Here, convection is the dominant mechanism inside the cavity. One can observe a small difference in the Nusselt numbers when the thermal conductivity $k = 10$ and $k = 100$ but a large difference when $k = 1$. The average heat transfer increases as the thermal conductivity increases, which is more pronounced for higher values. On the other hand, the heat transfer for water-based nanofluids containing alumina NP is more efficient than the base fluid, resulting from the higher thermal conductivity of the two solid NPs. The solid volume fraction increase governs the heat transfer increase. First of all, the convection heat transfer becomes more dominant while the Rayleigh number augments, but efficient thermal conductivity is attained. Moreover, the nanofluids' viscosity effects also become significant. Increasing the volume fraction of NPs directly affects the heat transfer where the behavior of the responsible factors is as follows. The first one reduces the heat transfer rate, which could be expressed in the nanofluid's viscosity increase. The second factor improves the thermal exchange at the point of augmenting the nanofluid's thermal conductivity. From what was said previously, it is clear that the viscosity effect is less operative than that of the conductivity. On the other hand, the heat transfer rate has a proportional relation to the volume fraction. We can note that the highest values of the Nu_m are obtained for $Ra = (10^4, 10^5)$ shown in case 1 ($a = 0.1, b = 0.4, h = 0.5$). For $Ra = 10^6$ it is obtained both in case 5 ($a = 0.2, b = 0.3, h = 0.5$) and case 2 ($a = 0.2, b = 0.4, h = 0.5$). Furthermore, the lowest values of Nu_m are obtained for case 3 ($a = 0.3, b = 0.4, h = 0.5$) and case 5 ($a = 0.2, b = 0.1, h = 0.5$).

Figure 7 demonstrates the evolution of the S_{tot} with ϕ of Al_2O_3 NPs and for various Ra (10^4 – 10^6) at different thermal conductivities and body dimensions. The total entropy generation decreases as the NPs increase for all cases, but for $Ra = 10^4$, the S_{tot} increases as the NPs increase for all cases, since a greater number of NPs is added, the predictable result is an increased viscosity and thermal conductivity. NPs presence has two contrary effects on the entropy generation. The first one is expressed in the heat transfer improvement, which decreases the temperature gradient and reduces entropy generation. Other than that, friction losses increase with the nanofluid viscosity increase, which leads to an entropy generation increase. Entropy at a higher Ra number is reduced significantly by NPs presence. A greater number of NPs increases the viscosity and the thermal conductivity. As noticed, when Ra is less than 10^5 , the dominant effect in decreasing the total entropy generation is the Ra value. However, the Ra number is more distinctive in nanofluid than the base fluid. An Ra increase introduces an entropy generation increase because of the heat transfer flow augmentation and,

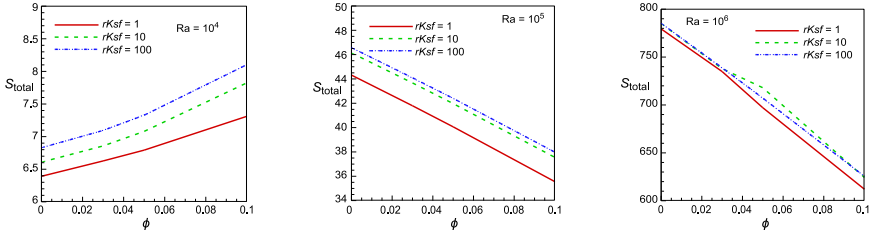
a) Case 2 ($a = 0.2, b = 0.4, h = 0.5$)



b) Case 3 ($a = 0.3, b = 0.4, h = 0.5$)



c) Case 4 ($a = 0.2, b = 0.1, h = 0.5$)



d) Case 5 ($a = 0.2, b = 0.3, h = 0.5$)

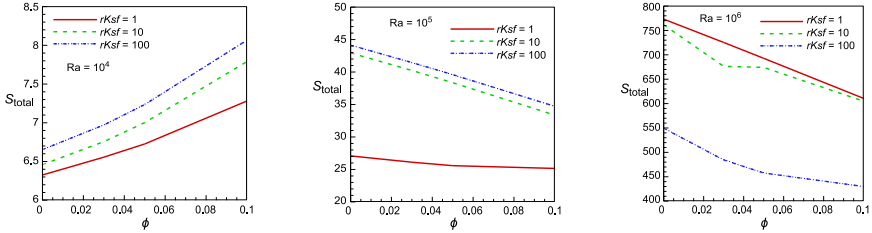
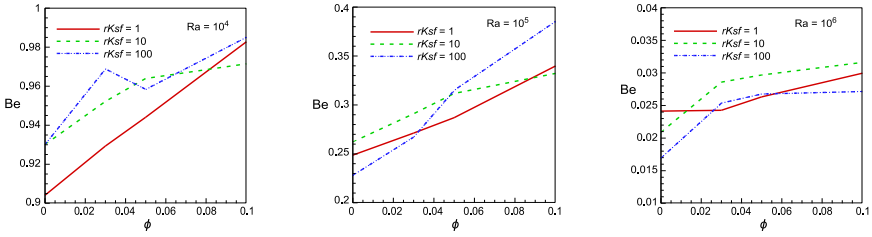


FIG. 7. The S_{tot} evolution with ϕ for various Ra, thermal conductivities, and geometries.

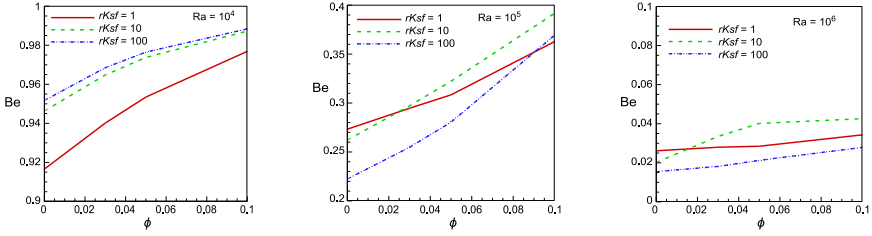
consequently, a higher temperature gradient. In other words, entropy generation obtained from heat transfer concentrates along the walls. We can conclude that the highest values of S_{tot} are obtained for $Ra = (10^4, 10^5)$ case 4 ($a = 0.2, b = 0.1, h = 0.5$) and for $Ra = 10^6$ case 2 ($a = 0.2, b = 0.4, h = 0.5$) and case 4 ($a = 0.2, b = 0.1, h = 0.5$), and low-ranking values of the total entropy generation are obtained for case 3 ($a = 0.3, b = 0.4, h = 0.5$).

Figure 8 demonstrates the Be evolution with the volume fraction of Al_2O_3 NPs and for various Ra (10^4 – 10^6), thermal conductivities and body dimensions.

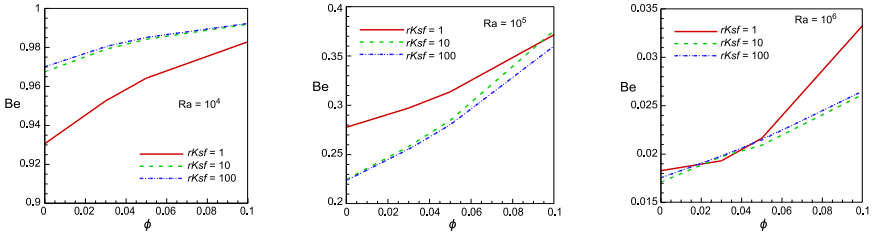
a) Case 1 ($a = 0.1, b = 0.4, h = 0.5$)



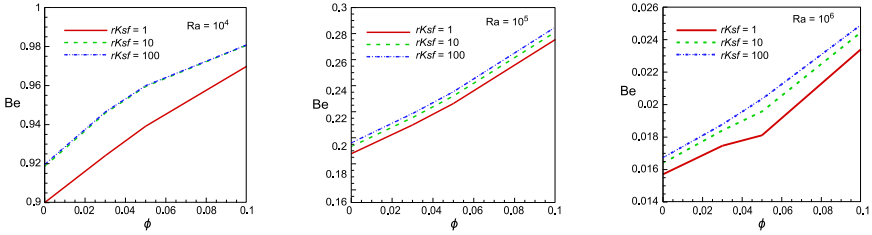
b) Case 2 ($a = 0.2, b = 0.4, h = 0.5$)



c) Case 3 ($a = 0.3, b = 0.4, h = 0.5$)



d) Case 4 ($a = 0.2, b = 0.1, h = 0.5$)



e) Case 5 ($a = 0.2, b = 0.3, h = 0.5$)

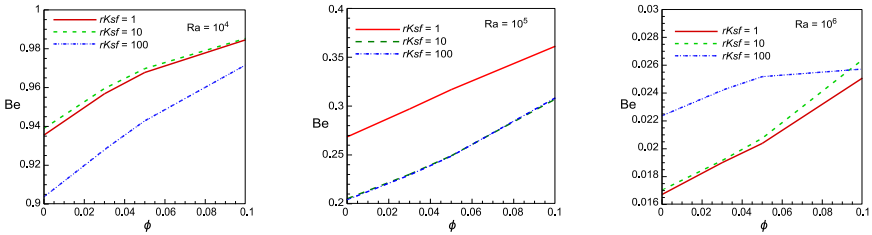


FIG. 8. The Be evolution with ϕ for various Ra, thermal conductivities, and geometries.

The Be augments with the increasing volume fraction of Al_2O_3 NPs in all of the cases studied and increased the viscosity of the working fluid and the thermal conductivity, so that the heat transfer irreversibility mode is dominant relative to that of viscous irreversibility. An increased flow velocity adds to the Be reduction, corresponding to the fluid friction irreversibility effect increase in all the cases. Remarkably, this increase in Be is obtained at the same time as the total entropy generation quickly increases. Additionally, we observe that the uppermost and low-ranking values of Be are obtained for case 3 ($a = 0.3$, $b = 0.4$, $h = 0.5$) and case 4 ($a = 0.2$, $b = 0.1$, $h = 0.5$), respectively.

5. CONCLUSIONS

The present paper presented an approach for heat transfer in a square cavity with a body located at the left wall filled with a Al_2O_3 /water nanofluid for different geometries. The discussed results were obtained via the Fortran program for numerous experiments. The results show that the total entropy generation increase is related to the Ra number increase. Besides, the NPs volume fraction increase led to the Nu number increase and the total entropy generation decrease. The Be number increased because of the thermal conductivity ratio and NPs volume fraction augmentation. Dimensional variation of the body directly affected the Nu number, which involved heat transfer.

REFERENCES

1. ALLOUI Z., VASSEUR P., REGGIO M., Natural convection of nanofluids in a shallow cavity heated from below, *International Journal of Thermal Sciences*, **50**(3): 385–393, 2011, doi: 10.1016/j.ijthermalsci.2010.04.006.
2. ZHANG Y., LI L., MA H.B., YANG M., Effect of Brownian and thermophoretic diffusions of nanoparticles on nonequilibrium heat conduction in a nanofluid layer with periodic heat flux, *Numerical Heat Transfer, Part A: Applications: An International Journal of Computation and Methodology*, **56**(4): 325–341, 2009, doi: 10.1080/10407780903163876.
3. JOU R.-Y., TZENG S.-C., Numerical research of nature convective heat transfer enhancement filled with nanofluids in rectangular enclosures, *International Communications in Heat and Mass Transfer*, **33**(6): 727–736, 2006, doi: 10.1016/j.icheatmasstransfer.2006.02.016.
4. HERIS Z.S., ESFAHANY M.N., ETEMAD G., Numerical investigation of nanofluid laminar convection heat transfer through a circular tube, *Numerical Heat Transfer, Part A: Applications: An International Journal of Computation and Methodology*, **52**(11): 1043–1058, 2007, doi: 10.1080/10407780701364411.
5. ABU-NADA E., Investigation of entropy generation over a backward facing step under bleeding conditions, *Energy Conversion and Management*, **49**(11): 3237–3242, 2008, doi: 10.1016/j.enconman.2007.10.031.

6. KIM S.S., BAEK S.W., Radiation affected compressible turbulent flow over a backward facing step, *International Journal of Heat and Mass Transfer*, **39**(16): 3325–3332, 1996, doi: 10.1016/0017-9310(96)00046-4.
7. GUERRERO J.S.P., COTTA R.M., Benchmark integral transform results for flow over a backward-facing step, *Computers & Fluids*, **25**(5): 527–540, 1996, doi: 10.1016/0045-7930(96)00005-9.
8. BENARD N., GARRIDO P.S., BONNET J.P., MOREAU E., Control of the coherent structure dynamics downstream of a backward facing step by DBD plasma actuator, *International Journal of Heat and Fluid Flow*, **61**(Part A): 158–173, 2016, doi: 10.1016/j.ijheatfluidflow.2016.04.009.
9. CHANG T.S., TSAY Y.L., Natural convection heat transfer in an enclosure with a heated backward step, *International Journal of Heat and Mass Transfer*, **44**(20): 3963–3971, 2001, doi: 10.1016/S0017-9310(01)00035-7.
10. RAMŠAK M., Conjugate heat transfer of backward-facing step flow: A benchmark problem revisited, *International Journal of Heat and Mass Transfer*, **84**: 791–799, 2015, doi: 10.1016/j.ijheatmasstransfer.2015.01.067.
11. NIEMANN M., FRÖHLICH J., Buoyancy-affected backward-facing step flow with heat transfer at low Prandtl number, *International Journal of Heat and Mass Transfer*, **101**: 1237–1250, 2016, doi: 10.1016/j.ijheatmasstransfer.2016.05.137.
12. XU F., GAO Z., MING X., XIA L., WANG Y., SUN W., MA R., The optimization for the backward-facing step flow control with synthetic jet based on experiment, *Experimental Thermal and Fluid Science*, **64**: 94–107, 2015, doi: 10.1016/j.expthermflusci.2015.02.014.
13. KHERBEET A.S., MOHAMMED H.A., SALMAN B.H., AHMED H.E., ALAWI O.A., RASHIDI M.M., Experimental study of nanofluid flow and heat transfer over microscale backward- and forward-facing steps, *Experimental Thermal and Fluid Science*, **65**: 13–21, 2015, doi: 10.1016/j.expthermflusci.2015.02.023.
14. MRAMOR K., VERTNIK R., ŠARLER B., Simulation of laminar backward facing step flow under magnetic field with explicit local radial basis function collocation method, *Engineering Analysis with Boundary Elements*, **49**: 37–47, 2014, doi: 10.1016/j.engana-bound.2014.04.013.
15. STATNIKOV V., BOLGAR I., SCHARNOWSKI S., MEINKE M., KÄHLER C.J., SCHRÖDER W., Analysis of characteristic wake flow modes on a generic transonic backward-facing step configuration, *European Journal of Mechanics – B/Fluids*, **59**: 124–134, 2016, doi: 10.1016/j.euromechflu.2016.05.008.
16. AGHAKHANI S., PORDANJANI A.H., AFRAND M., SHARIFPUR M., MEYER J.P., Natural convective heat transfer and entropy generation of alumina/water nanofluid in a tilted enclosure with an elliptic constant temperature: applying magnetic field and radiation effects, *International Journal of Mechanical Sciences*, **174**: 105470, 2020, doi: 10.1016/j.ijmecsci.2020.105470.
17. ALNAQI A.A., AGHAKHANI S., PORDANJANI A.H., BAKHTIARI R., ASADI A., TRAN M.-D., Effects of magnetic field on the convective heat transfer rate and entropy generation of a nanofluid in an inclined square cavity equipped with a conductor fin: Considering the radiation effect, *International Journal of Heat and Mass Transfer*, **133**: 256–267, 2019, doi: 10.1016/j.ijheatmasstransfer.2018.12.110.
18. BAGHSAZ S., REZANEJAD S., MOGHIMI M., Numerical investigation of transient natural convection and entropy generation analysis in a porous cavity filled with nanofluid con-

- sidering nanoparticles sedimentation, *Journal of Molecular Liquids*, **279**: 327–341, 2019, doi: 10.1016/j.molliq.2019.01.117.
19. BEZI S., SOUAYEH B., CHEIKH N.B., BEYA B.B., Numerical simulation of entropy generation due to unsteady natural convection in a semi-annular enclosure filled with nanofluid, *International Journal of Heat and Mass Transfer*, **124**: 841–859, 2018, doi: 10.1016/j.ijheatmasstransfer.2018.03.109.
 20. BONDAREVA N.S., SHEREMET M.A., ÖZTOP H.F., HAMDEH N.A., Entropy generation due to natural convection of a nanofluid in a partially open triangular cavity, *Advanced Powder Technology*, **28**(1): 244–255, 2017, doi: 10.1016/j.appt.2016.09.030.
 21. CHO C.-C., Heat transfer and entropy generation of mixed convection flow in Cu-water nanofluid-filled lid-driven cavity with wavy surface, *International Journal of Heat and Mass Transfer*, **119**: 163–174, 2018, doi: 10.1016/j.ijheatmasstransfer.2017.11.090.
 22. DOGONCHIA A.S., SEYYEDIB S.M., TILEHNOEEA M.H., CHAMKHA A.J., GANJI D.D.D., Investigation of natural convection of magnetic nanofluid in an enclosure with a porous medium considering Brownian motion, *Case Studies in Thermal Engineering*, **14**: 100502, 2019, doi: 10.1016/j.csite.2019.100502.
 23. DORMOHAMMADI R., FARZANEH-GORD M., EBRAHIMI-MOGHADAM A., AHMADI M.H., Heat transfer and entropy generation of the nanofluid flow inside sinusoidal wavy channels, *Journal of Molecular Liquids*, **269**: 229–240, 2018, doi: 10.1016/j.molliq.2018.07.119.
 24. HASHIM I., ALSABERY A.I., SHEREMET M.A., CHAMKHA A.J., Numerical investigation of natural convection of Al_2O_3 -water nanofluid in a wavy cavity with conductive inner block using Buongiorno's two-phase model, *Advanced Powder Technology*, **30**(2): 399–414, 2019, doi: 10.1016/j.appt.2018.11.017.
 25. KHAKRAH H., HOOSHMAND P., JAMALABADI M.Y.A., AZAR S., Thermal lattice Boltzmann simulation of natural convection in a multi-pipe sinusoidal-wall cavity filled with Al_2O_3 -EG nanofluid, *Powder Technology*, **356**: 240–252, 2019, doi: 10.1016/j.powtec.2019.08.013.
 26. RAHIMI A., SEPEHR M., LARICHE M.J., KASAEIPOOR A., MALEKSHAH E.H., KOLSI L., Entropy generation analysis and heatline visualization of free convection in nanofluid (KKL model-based)-filled cavity including internal active fins using lattice Boltzmann method, *Computers & Mathematics with Applications*, **75**(5): 1814–1830, 2018, doi: 10.1016/j.camwa.2017.12.008.
 27. RAHIMI A., SEPEHR M., LARICHE M.J., MESBAH M., KASAEIPOOR A., MALEKSHAH E.H., Analysis of natural convection in nanofluid-filled H-shaped cavity by entropy generation and heatline visualization using lattice Boltzmann method, *Physica E: Low-dimensional Systems and Nanostructures*, **97**: 347–362, 2018, doi: 10.1016/j.physe.2017.12.003.
 28. SELIMEFENDIGIL F., ÖZTOP H.F., Effects of conductive curved partition and magnetic field on natural convection and entropy generation in an inclined cavity filled with nanofluid, *Physica A: Statistical Mechanics and its Applications*, **540**: 123004, 2020, doi: 10.1016/j.physa.2019.123004.
 29. SHEIKHOESLAMI M., ÖZTOP H.F., MHD free convection of nanofluid in a cavity with sinusoidal walls by using CVFEM, *Chinese Journal of Physics*, **55**(6): 2291–2304, 2017, doi: 10.1016/j.cjph.2017.09.006.
 30. SHEREMET M.A., POP I., ÖZTOP H.F., HAMDEH N.A., Natural convective heat transfer and nanofluid flow in a cavity with top wavy wall and corner heater, *Journal of Hydrodynamics*, **28**(5): 873–885, 2016, doi: 10.1016/S1001-6058(16)60688-1.

31. AMINOSADATI S.M., GHASEMI B., Natural convection cooling of a localised heat source at the bottom of a nanofluid-filled enclosure, *European Journal of Mechanics – B/Fluids*, **28**(5): 630–640, 2009, doi: 10.1016/j.euromechflu.2009.05.006.
32. HASSAN M., MEBAREK-LOUDINA F., FAISAL A., GHAFAR A., ISMAIL A.I., Thermal energy and mass transport of shear thinning fluid under effects of low to high shear rate viscosity, *International Journal of Thermofluids*, **15**: 100176, 2022, doi: 10.1016/j.ijft.2022.100176.
33. SHAFIQ A., MEBAREK-LOUDINA F., SINDHU T.N., RASSOL G., Sensitivity analysis for Walters-B nanoliquid flow over a radiative Riga surface by RSM, *Scientia Iranica*, **29**(3): 1236–1249, 2022, doi: 10.24200/sci.2021.58293.5662.
34. REDDY Y.D., MEBAREK-LOUDINA F., GOUD B.S., ISMAIL A.I., Radiation velocity and thermal slips effect toward MHD boundary layer flow through heat and mass transport of Williamson nanofluid with porous medium, *Arabian Journal for Science and Engineering*, **47**(12): 16355–16369, 2022, doi: 10.1007/s13369-022-06825-2.
35. DHIF K., MEBAREK-LOUDINA F., CHOUF S., VAIDYA H., CHAMKHA A.J., Thermal analysis of the solar collector cum storage system using a hybrid-nanofluids, *Journal of Nanofluids*, **10**(4): 616–626, 2021, doi: 10.1166/jon.2021.1807.
36. MEBAREK-LOUDINA F., Numerical modeling of the hydrodynamic stability in vertical annulus with heat source of different lengths, *Engineering Science and Technology, an International Journal*, **20**(4): 1324–1333, 2017, doi: 10.1016/j.jestch.2017.08.003.
37. MEBAREK-LOUDINA F., Convective heat transfer of Titania nanofluids of different base fluids in cylindrical annulus with discrete heat source, *Heat Transfer – Asian Research*, **48**(1): 135–147, 2019, doi: 10.1002/htj.21375.
38. CHABANI I., MEBAREK-LOUDINA F., VAIDYA H., ISMAIL A.I., Numerical analysis of magnetic hybrid nano-fluid natural convective flow in an adjusted porous trapezoidal enclosure, *Journal of Magnetism and Magnetic Materials*, **564**(2): 170142, 2022, doi: 10.1016/j.jmmm.2022.170142.
39. MARZOUGUI S., MEBAREK-LOUDINA F., MAGHERBI M., MCHIRGUI A., Entropy generation and heat transport of Cu-water nanoliquid in porous lid-driven cavity through magnetic field, *International Journal of Numerical Methods for Heat & Fluid Flow*, **32**(6): 2047–2069, 2022, doi: 10.1108/HFF-04-2021-0288.
40. BRINKMAN H.C., The viscosity of concentrated suspensions and solution, *The Journal of Chemical Physics*, **20**(4): 571–581, 1952, doi: 10.1063/1.1700493.
41. MAXWELL J., *A Treatise on Electricity and Magnetism*, 2nd ed., Oxford University Press, Cambridge, UK, 1904.
42. PATANKAR S.V., *Numerical Heat Transfer and Fluid Flow*, McGraw-Hill, New York, 1980.

Received February 11, 2022; accepted version January 20, 2023.



Copyright © 2023 The Author(s).

This is an open-access article distributed under the terms of the Creative Commons Attribution-ShareAlike 4.0 International (CC BY-SA 4.0 <https://creativecommons.org/licenses/by-sa/4.0/>) which permits use, distribution, and reproduction in any medium, provided that the article is properly cited. In any case of remix, adapt, or build upon the material, the modified material must be licensed under identical terms.